Journal of the Mechanics and Physics of Solids 59 (2011) 1613–1622

Contents lists available at ScienceDirect

Journal of the Mechanics and Physics of Solids

journal homepage: www.elsevier.com/locate/jmps

The interlayer shear effect on graphene multilayer resonators

Yilun Liu, Zhiping Xu, Quanshui Zheng*

Department of Engineering Mechanics and Center for Nano and Micro Mechanics, Tsinghua University, Beijing 100084, China

ARTICLE INFO

Article history:
Received 3 December 2010
Received in revised form
14 April 2011
Accepted 15 April 2011
Available online 21 April 2011

Keywords:
Multilayer graphene nanostrips
Resonant frequencies
Molecular dynamics (MD)
Multibeam shear model (MBSM)
Nanomechanical devices

ABSTRACT

Graphene nanostrips with single or few layers can be used as bending resonators with extremely high sensitivity to environmental changes. In this paper we report molecular dynamics (MD) simulation results on the fundamental and secondary resonant frequencies f of cantilever graphene nanostrips with different layer number n and different nanostrip length L. The results deviate significantly from the prediction of not only the Euler–Bernoulli beam theory ($f \propto nL^{-2}$), but also the Timoshenko's model. Since graphene nanostrips have extremely high intralayer Young's modulus and ultralow interlayer shear modulus, we propose a multibeam shear model (MBSM) that neglects the intralayer stretch but accounts for the interlayer shear. The MBSM prediction of the fundamental and secondary resonant frequencies f can be well expressed in the form $f-f_{mono} \propto [(n-1)/n]^b L^{-2(1-b)}$, where f_{mono} denotes the corresponding resonant frequency as the layer number is 1, with $b=0.61$ and 0.77 for the fundamental and secondary resonant modes. Without any additional parameters fitting, the prediction from MBSM agrees excellently with the MD simulation results. The model is thus of importance for designing multilayer graphene nanostrips based applications, such as resonators, sensors and actuators, where interlayer shear has apparent impacts on the mechanical deformation, vibration and energy dissipation processes therein.

1. Introduction

Two-dimensional graphene monolayer, where carbon atoms are bonding together through in-plane sp^2 bonds, features unique physical and chemical properties including isotropic planar elasticity with ultra-high in-plane stiffness and strength and Dirac fermions electronic structures (Novoselov et al., 2005; Zhang et al., 2005). Its thermal conductivity and mechanical stiffness/strength can reach the in-plane values of its bulk counterpart, graphite, and surpass most of the other engineering materials (Balandin et al., 2008; Gómez-Navarro et al., 2007; Lee et al., 2008; Stankovich et al., 2006; Xu, 2009). According to its high stiffness and perfect lattice structure extending to macroscopic length scales, graphene sheet holds great promises in developing nano-electromechanical devices featuring resonant frequencies beyond 100 MHz (Bunch et al., 2007; Chen et al., 2009; Robinson et al., 2010) and simultaneously quality-factors Q up to 10^4 (Chen et al., 2009). The rapid development of graphene synthesis and transfer techniques (Lee et al., 2008; Li et al., 2009) recently even promotes fabrication of graphene-based nano-devices and more proposed applications thus become feasible.

Frequencies for the eigen-modes are of extremely importance for sensors and actuators based on a resonant mechanism, as the changes in their resonant frequencies under external cues such as adsorption, contamination and electromagnetic field, are usually utilized as characterization of the cue amplitudes (Ekinci, 2005; Ekinci et al., 2004;

* Corresponding author.
E-mail address: zhengqs@tsinghua.edu.cn (Q. Zheng).

0022-5096/$ - see front matter © 2011 Elsevier Ltd. All rights reserved.
doi:10.1016/j.jmps.2011.04.014

Huang et al., 2003; Poncharal et al., 1999). The resonant vibration of bending modes of multilayered graphene nanostrips, not only features very high frequencies and large transverse displacement because of their thickness of a few atoms, but also can be engineered by tuning both the number of graphene layers and geometry of nanostrips (size, shape, etc.). Thus for optimal design of graphene nanostrip-based electromechanical devices, it is necessary to understand relationship between the transverse vibration dynamics, corresponding resonant frequencies and the beam structures. In contrast to the conventional beams in nano or micromechanical devices, such as silicon carbide, zinc oxide nanowires and carbon nanotubes at the small deformation regime (Huang et al., 2003; Ke et al., 2005; Pugno, 2005), where Euler–Bernoulli beam theory gives quantitatively accurate prediction, novel phenomena and effects are recently observed in graphene structures, such as the out-of-plane deformation and localized ripple of the graphene sheet. In bending deformation, these effects can modify the mechanical properties (Fasolino et al., 2007; Xu and Buehler, 2010), charge distribution and its electron transport properties (Bolotin et al., 2008; Gibertini et al., 2010).

Graphene, only one atom thick, is the thinnest material in the nature. This leads to exceptional mechanical properties of graphene, such as extensibility up to a strain of 20% (Lee et al., 2008; Meyer et al., 2007; Xu, 2009). The in-plane stiffness and strength of graphene are exceptionally high, on the order of 1 TPa and 200 GPa, respectively (Gómez-Navarro et al., 2007; Lee et al., 2008). On the other hand the graphene can also be very flexible as the out-of-plane deformation amplitude can be extremely large for large-scale sheet because of its high aspect ratio. Surface ripples are also an intrinsic feature of suspended graphene sheet induced by thermal fluctuation or local defects (Meyer et al., 2007). A regular one- or two-dimensional ripple texture can be easily generated in a suspended graphene film by different thermal strains in the graphene and interface stress between the graphene and underlying substrate (Bao et al., 2009; Xu and Buehler, 2010). Moreover, a supported graphene can follow the substrate to generate complicated morphology (Li and Zhang, 2010). The mechanical properties of a single layer or multilayer graphene can be described by continuum shell models (Arroyo and Belytschko, 2002; Huang et al., 2010; Huang et al., 2006; Wang et al., 2005; Yakobson et al., 1996). A unique feature of the multilayered graphene structures is the extreme anisotropy between interlayer shear and intralayer tensile modulus and strength (Wang and Zheng, 2007), which is utilized in several types of nanomechanical devices (Shi et al., 2010a, b; Shi et al., 2009; Xu et al., 2008; Zheng and Jiang, 2002). In order to describe the mechanical properties of multilayer graphene based materials, such as multi-walled carbon nanotube and multilayer graphene sheets, the interlayer van der Waals interaction has been incorporated into the continuum shell models of the single layer graphene (Arroyo and Belytschko, 2005; He et al., 2005; Liew et al., 2006; Ru, 2001). However the existing continuum models for multilayer graphene fail to consider the shear energy between the graphene layers as the discrete graphene lattice registry is not included in the continuum models. As the very small thickness of the graphene leads to a very small bending rigidity, the interlayer shear energy may play a very important role in bending and vibration of multilayer graphene sheets and must be considered in the related continuum models.

In multilayer graphene sheets, unlike conventional bulk materials that are widely used in micro-electromechanical devices, the interlayer van der Waals binding is very weak that enables flexibility for interlayer shear deformation or relative sliding. Self-retracting behavior is discovered in extracted graphite microflakes from substrate, indicating an extremely low resistance against shear loads and representing a new mode of pulling-retracting motion (Zheng et al., 2008). Similar self-retracting behavior is also found in multi-walled carbon nanotubes with the interlayer shear strength estimated as 0.3–0.48 MPa (Cumings and Zettl, 2000; Yu et al., 2000a; Yu et al., 2000b). This unique feature not only provides a highly mobile interface between neighboring graphene sheets that can be in purpose designed for use in mechanical devices, but also has dramatic effects on the physical and chemical properties of multilayer graphene sheets as a bulk material. However, these issues are not well addressed in earlier works studying the dynamical behaviors of graphene resonators (Bunch et al., 2007; Chen et al., 2009; Robinson et al., 2008). In general, effects of the interlayer shear on the vibrational behavior of multilayer graphene beam are still not clarified. In order to investigate the effects of interlayer shear on their resonant performance, we perform molecular dynamics (MD) simulations of cantilever beams consisting of various numbers of graphene layers. According to the simulation results, negligible in-plane tension is involved in the bending motion of multilayer graphene beam, thus we also pursue theoretical analysis based on the tension-free assumption.

2. Molecular dynamics simulations

In the MD simulations we use Dreiding force-field to describe both the intralayer and interlayer interactions between carbon atoms (Mayo et al., 1990). The parameters in the potential function are validated by correctly characterizing the structural and mechanical properties of carbon nanostructures (Guo et al., 1991; Rivera et al., 2003; Xu et al., 2008). The software GROMACS (Lindahl et al., 2001) is used for all the MD simulations. The graphene nanostrips investigated here have rectangular cross-sections with a fixed width of 2 nm but different heights as can be calculated by their layer number n and interlayer distance h. The lengths of the strips ranging from 8 to 16 nm are investigated in the simulations.

After structural relaxation, we apply a displacement of 1 nm to the free end of each cantilevered nanostrip at the beginning of the simulation to initialize a transverse vibration. The system then evolves in a NVE ensemble. The equations of motion are integrated numerically using the Velocity-Verlet algorithm with a time step of 1 fs. The atomic structures of the multilayer graphene nanostrips at initiation are illustrated in Fig. 1(a), showing a remarkable shear deformation at the free end of each multilayer graphene cantilever under investigation. The free end transversal motion of the strips is tracked, as plotted in Fig. 1(b). We see that the vibration sustains without significant energy dissipation in the duration of

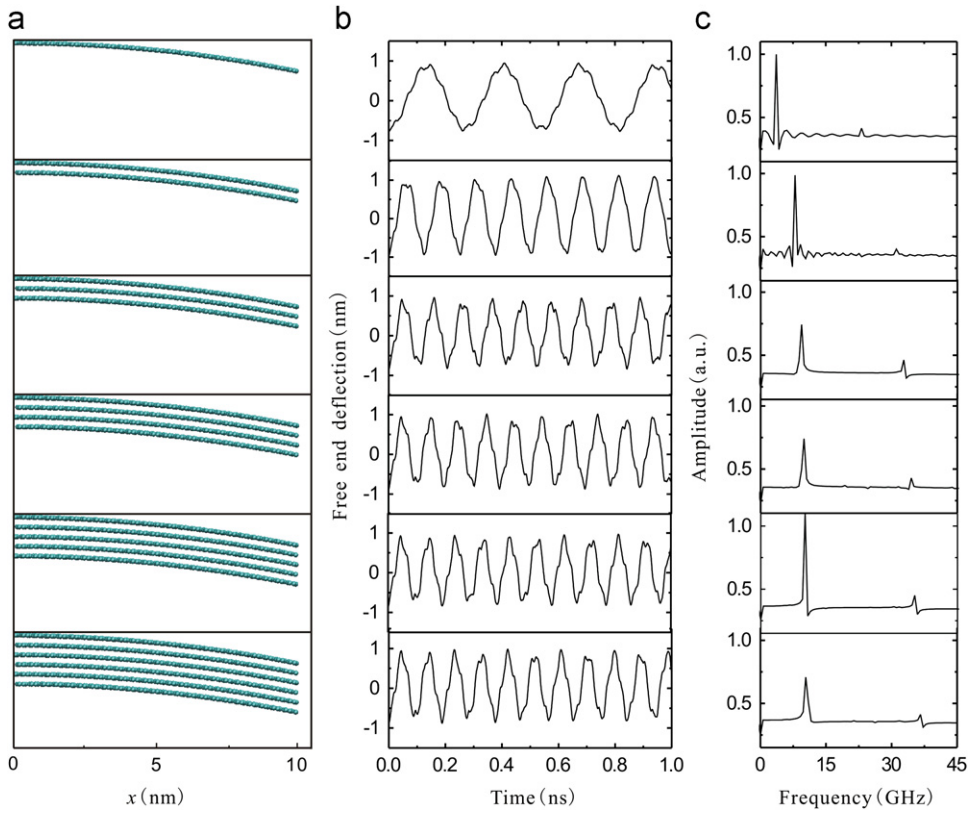

Fig. 1. The transversal vibration motion of the graphene cantilever nanostrips. (a) Atomic structures of the cantilevers consisting of one through six layers, with a width of 2 nm and length of 10 nm. Initial amplitude of the free-end deflection is 1 nm. (b) Free-end displacements of the corresponding graphene nanostrips. (c) Resonant frequencies of the corresponding cantilevered graphene nanostrips resulted from fast Fourier transformation of (b).

one nanosecond. We also see that the displacement–time curve deviates from ideal sinusoidal function, featuring numerous corrugations that result from local ripples in the graphene sheets. This phenomenon is unique for fewer-layer graphene sheets in which higher-order beam-like modes with much shorter wavelength are immediately excited in addition to the first-order mode as initialized. The fast Fourier transformation (FFT) results are shown in Fig. 1(c), clearly indicating domination of the fundamental resonance, coupled by the secondary resonance.

From Fig. 1(c) we can see that the fundamental and secondary resonant frequencies f shift not much when the graphene layer number n exceeds two. To show more clearly the f–n dependence, we plot the fundamental and secondary frequencies obtained from MD simulations in Fig. 2(a) and (c) as red hollow circles, respectively. We also investigate the fundamental and secondary frequency–length relationships of multilayer graphene nanostrips by using MD simulations. Resonant frequencies are calculated for nanostrips with length L, ranging from 8 to 16 nm. The red hollow circles plotted in Fig. 2(b) and (d) represent the simulated results of three-layer graphene nanostrips.

3. Multibeam shear model

3.1. Euler–Bernoulli model

Due to their large length-to-thickness ratios, typical thin beams are well described by classical Euler–Bernoulli beam model (EBM). For a cantilever beam with a uniform rectangular cross-section of thickness H and width b made of a homogeneous linear elastic material, its resonant frequencies are known to be

$$f = \frac{\beta^2}{2\pi L^2}\sqrt{\frac{EI}{\rho A}}, \tag{1}$$

where E and ρ are Young's modulus and mass density of the material, $A=bH$ and $I=bH^3/12$ are cross-section area and area inertia moment and β is the resonant mode parameter that is one of the solutions of equation

$$1+\cosh\beta\cos\beta=0, \tag{2}$$

giving the values of $\beta=1.875$, 4.694, 7.855, …, for the leading resonant modes.

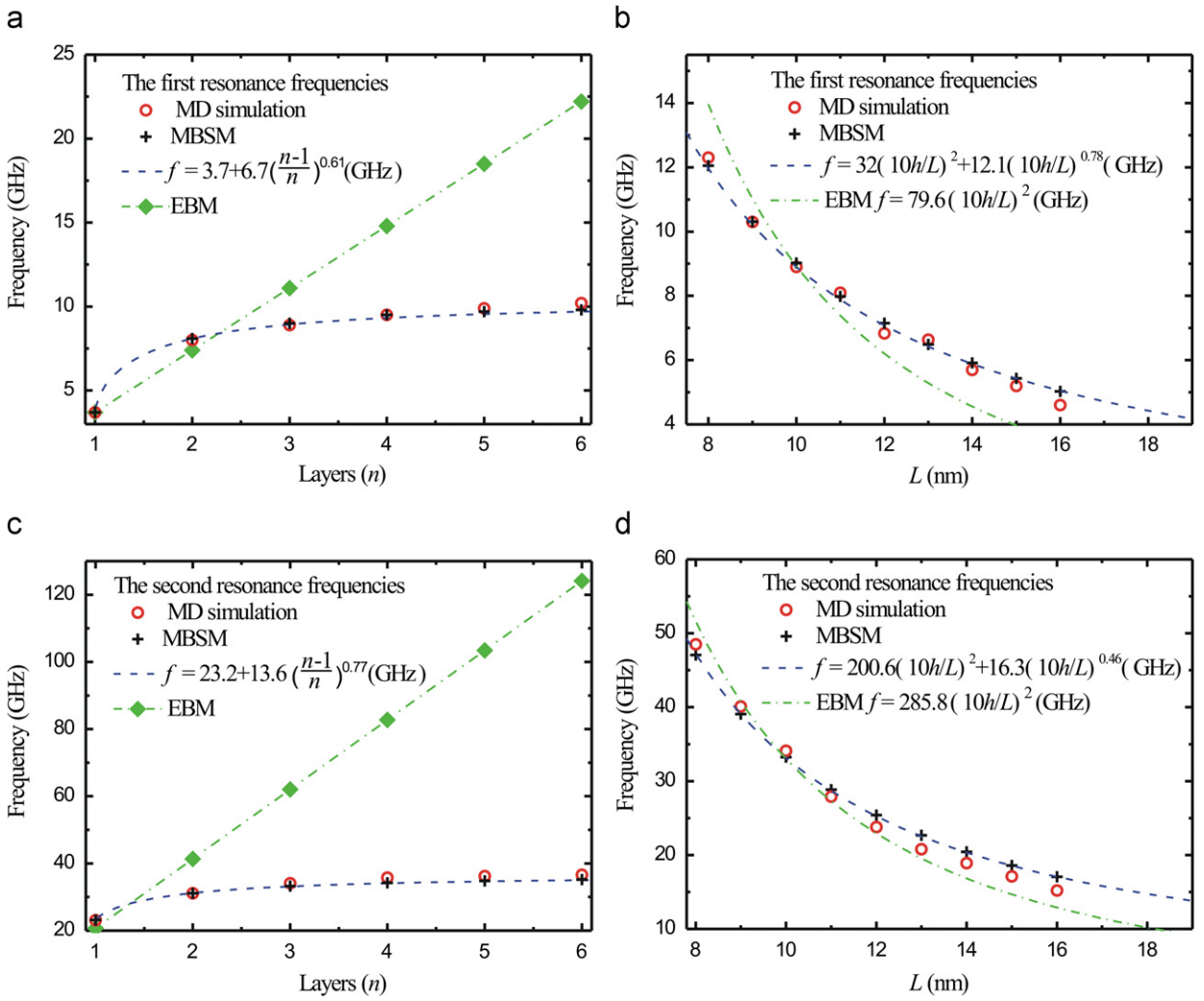

Fig. 2. The fundamental and secondary resonant frequencies of graphene cantilever nanostrips with different layers and different lengths. (a) Fundamental frequencies of graphene cantilever nanostrips consisting of one through six layers. Different results are from empirical molecular dynamics (MD) simulations (red hollow circles), the relation of $f=3.7+6.7[(n-1)/n]^{0.61}$ (blue dashed line), Euler–Bernoulli beam model (EBM) prediction (green squares) and multibeam shear model (MBSM) prediction (black crosses). (b) Scaling laws of the fundamental resonant frequencies of three-layer graphene cantilever nanostrips. Different results are from MD simulation (hollow circles), the relation of $f=32(10h/L)^2+12.1(10h/L)^{0.78}$ (blue dashed line), MBSM prediction (crosses) and EBM prediction (green dash-dotted line). (c) and (d) The secondary resonant frequencies with different layers and lengths, with the same representations as (a) and (b), respectively. (For interpretation of the references to color in this figure legend, the reader is referred to the web version of this article.)

If EBM is applied to our studied n-layer graphene beams, we have $H=nh$, where $h=0.335$ nm is the interlayer spacing. Thus, (1) can be reformulated into the following form:

$$f = \frac{\beta^2}{2\pi L^2}\sqrt{\frac{D_{\text{bend}}}{\rho h}}n = f_{\text{mono}}n, \tag{3}$$

with

$$f_{\text{mono}} = \frac{\beta^2}{2\pi L^2}\sqrt{\frac{D_{\text{bend}}}{\rho h}}, \tag{4}$$

where D_{bend} is the bending rigidity of a monolayer graphene of unit width, and f_{mono} the resonant frequency of a monolayer graphene cantilever beam. Thus, EBM gives a linear dependence upon the layer number $f \propto n$ and a scaling law $f \propto L^{-2}$. While if the interlayer interaction is extremely weak and graphene layers vibrate independently, the frequencies f then apparently have no dependence on the number of layers n. To view the departures of the EBM prediction f from the MD simulation results for the fundamental and secondary resonant frequencies, we plot f versus n and L, respectively, in

Fig. 2(a), (b) and (c), (d) (green dash-dotted line), with the value $D_{\text{bend}}=3.42\times10^{-19}$ kgm^2 s^{-2} obtained by equating the fundamental resonant frequency of monolayer graphene cantilever obtained in our MD simulation into the EBM frequency relationship Eq. (4). The results reveal that EBM prediction deviates severely from the resonant behavior of multilayer graphene cantilever beams.

3.2. Multibeam shear model

In order to obtain some insights into this remarkable difference, we make such an analysis as introduced below. For the single-walled carbon nanotube, Yakobson et al., 1996 (see also Wang et al. (2005) and Chang and Gao (2003)) suggested that Young's modulus and thickness should be defined consistently as 5.5 TPa and 0.066 nm to enable the continuum shell model to accurately characterize the elastic response. It is notable that thickness 0.066 nm is one-fifth of the intuitive definition of graphene sheet thickness (interlayer distance in graphite or multi-walled carbon nanotubes). Thus, a more reasonable model for the graphene nanostrips should be a structure of multibeams. Indeed, from the vibrational deformation and motion of the multilayer graphene cantilever nanostrips (see, for example, Fig. 1(a)) we find that the weak interlayer van der Waals interaction cannot maintain the registry of carbon atoms in adjacent layers, and consequently the cantilevers cannot be considered as an integrated solid. Instead, we must incorporate the interlayer shear into our analysis for a more accurate estimation of the resonant frequencies of the multilayer graphene cantilever nanostrips. Here we propose a new model, which is denoted as multibeam shear model (MBSM). We firstly assume that every graphene layer behaves as a cantilever beam and then introduce a potential energy term accounting for the shear between neighboring graphene layers. From the MD simulation results we find that vibrations of all graphene layers are coherent, i.e. their displacements are almost the same. Thus we further make a simplification that every beam has the same transverse displacement w, and hence the same interlayer shear w', where superscript $'$ denotes spatial derivative along x direction in the beam contour.

Fig. 3 gives a schematic illustration of this model, in which the vertical massless rigid bars keep all the beams with the same w and the oblique massless springs establish proper interlayer shear elasticity, G. The beams are assumed to be inextensible as in-plane Young's modulus is too large compared to interlayer shear modulus (Kelly, 1981). The total potential energy of this multibeams system in equilibrium under a distributed transverse load q is thus equal to:

$$\prod(w)=n\frac{D_{\text{bend}}}{2}\int_0^L(w'')^2\mathrm{d}x+(n-1)\frac{D_{\text{shear}}}{2}\int_0^L(w')^2\mathrm{d}x-\int_0^L qw\mathrm{d}x, \tag{5}$$

where $D_{\text{shear}}=Gh$ is the graphene interlayer shear rigidity of unit width with G the interlayer shear modulus of graphene. The variation of Π with respect to w is derived as

$$\begin{aligned}\delta\prod(w)&=nD_{\text{bend}}\int_0^L w''\delta w''\,\mathrm{d}x+(n-1)D_{\text{shear}}\int_0^L w'\delta w'\,\mathrm{d}x-\int_0^L q\delta w\,\mathrm{d}x\\&=\int_0^L[nD_{\text{bend}}w''''-(n-1)D_{\text{shear}}w''-q]\delta w\,\mathrm{d}x+nD_{\text{bend}}w''\delta w'\big|_0^L-[nD_{\text{bend}}w'''-(n-1)D_{\text{shear}}w']\delta w\big|_0^L.\end{aligned} \tag{6}$$

Requiring $\delta\Pi=0$ yields the basic differential equation:

$$nD_{\text{bend}}w''''-(n-1)D_{\text{shear}}w''-q=0, \tag{7}$$

and substituting boundary conditions at the clamped end $\delta w(0)=0$ and $\delta w'(0)=0$ yields the boundary conditions at the free end:

$$\begin{aligned}&w''(L)=0,\\&D_{\text{bend}}w'''(L)-\frac{n-1}{n}D_{\text{shear}}w'(L)=0.\end{aligned} \tag{8}$$

Due to the interlayer shear, the transverse force boundary condition $(8)_2$ at the free end is different from that of a classical Euler–Bernoulli cantilever.

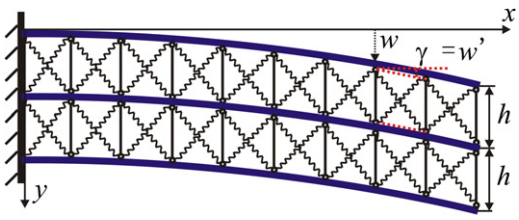

Fig. 3. Schematic illustration of MBSM model. The vertical massless rigid bars keep every beam having the same deflection and the oblique massless springs establish interlayer shear, where h is interlayer space, w is deflection of every beam and w' interlayer shear strain as indicated with dashed red line. (For interpretation of the references to color in this figure legend, the reader is referred to the web version of this article.)

To investigate free vibration of the system, the distributed load q is replaced by the inertial force $-n\rho h\ddot{w}$. The control equation now becomes:

$$D_{\text{bend}}w'''' - \frac{n-1}{n}D_{\text{shear}}w'' + \rho h\ddot{w} = 0. \tag{9}$$

For a harmonic vibration $w(x, t)=W(x)\sin\omega t$, it yields

$$\frac{\mathrm{d}^4W}{\mathrm{d}\xi^4} - \frac{n-1}{n}\frac{D_{\text{shear}}L^2}{D_{\text{bend}}}\frac{\mathrm{d}^2W}{\mathrm{d}\xi^2} - \frac{\rho hL^4\omega^2}{D_{\text{bend}}}W = 0, \tag{10}$$

where $\xi = x/L$ is the dimensionless coordinate. The general solution of Eq. (10) can be expressed as:

$$W = A_1\cosh\beta_+\xi + A_2\cos\beta_-\xi + A_3\beta_-\sinh\beta_+\xi + A_4\beta_+\sin\beta_-\xi, \tag{11}$$

where

$$\begin{aligned}
&\beta = \sqrt{\sqrt{\frac{\rho h}{D_{\text{bend}}}}\omega L},\\
&\eta = \frac{n-1}{2n}\frac{D_{\text{shear}}L^2}{D_{\text{bend}}},\\
&\beta_\pm = \sqrt{\sqrt{\beta^4+\eta^2}\pm\eta}.
\end{aligned} \tag{12}$$

By substituting the boundary conditions at the clamped end $W(0)=0$ and $W'(0)=0$ into general solution (11), we get relations $A_2=-A_1$ and $A_4=-A_3$. These relations, together with general solutions (11), are substituted into boundary Eqs. (8), leading to the following boundary equations:

$$\begin{aligned}
&(\beta_+^2\cosh\beta_+ + \beta_-^2\cos\beta_-)A_1 + \beta_-\beta_+(\beta_+\sinh\beta_+ + \beta_-\sin\beta_-)A_3 = 0,\\
&[(\beta_+^3\sinh\beta_+ - \beta_-^3\sin\beta_-) - 2\eta(\beta_+\sinh\beta_+ + \beta_-\sin\beta_-)]A_1 + [\beta_-\beta_+(\beta_+^2\cosh\beta_+ + \beta_-^2\cos\beta_-) - 2\eta\beta_+\beta_-(\cosh\beta_+ - \cos\beta_-)]A_3 = 0.
\end{aligned} \tag{13}$$

To obtain nonzero solutions of A_1 and A_3, the determinant of the coefficient eigen-matrix of (13) must be zero, viz

$$\beta_+^4 + \beta_-^4 - 2\eta(\beta_+^2 - \beta_-^2) - \beta_+\beta_-(\beta_+^2 - \beta_-^2 - 4\eta)\sin\beta_-\sinh\beta_+ + 2\eta(\beta_+^2 - \beta_-^2)\cos\beta_-\cosh\beta_+ + 2\beta_+^2\beta_-^2\cos\beta_-\cosh\beta_+ = 0, \tag{14}$$

Using the following identities:

$$\begin{aligned}
&\beta_+^2 - \beta_-^2 = 2\eta,\\
&\beta_+^2\beta_-^2 = \beta^4,\\
&\beta_-^4 + \beta_+^4 = 4\eta^2 + 2\beta^4.
\end{aligned} \tag{15}$$

we further simplify Eq. (14) into the following eigen-equation:

$$1 + \left(1 + 2\frac{\eta^2}{\beta^4}\right)\cosh\beta_+\cos\beta_- + \frac{\eta}{\beta^2}\sinh\beta_+\sin\beta_- = 0, \tag{16}$$

whenever $\eta=0$, Eq. (16) degenerates into Eq. (2), i.e. the eigen-equation for EBM.

3.3. Comparison of MBSM and MD simulation results

Unlike each solution of the mode parameter β from the Euler–Bernoulli model eigen-equation (2) is constant, the solutions of β from the MBSM eigen-equation (16) are functions of η. Since η has the range from 0 (as $n\to1$) to infinite (through enlarging L), it seems to be quite impossible to have simple analytical solutions $\beta(\eta)$. Instead, we can numerically get the exact leading solutions $\beta>0$ from Eq. (16). The results are plotted in Fig. 4 for the relationships between β^2 and η for the fundamental and secondary solutions. The dashed lines are the least-square fittings of the following power law

$$\beta^2 = \beta_{\text{mono}}^2 + a\eta^b, \tag{17}$$

with

$$\begin{aligned}
&\text{The fundamental resonant mode:}\quad \beta_{\text{mono}} = 1.875,\quad a = 1.36,\quad b = 0.61,\\
&\text{The secondary resonant mode:}\quad \beta_{\text{mono}} = 4.694,\quad a = 1.86,\quad b = 0.77.
\end{aligned} \tag{18}$$

Substituting (17) and $(12)_2$ into $(12)_1$ and noting $f=\omega/2\pi$, we obtain

$$f = f_{\text{mono}} + k\left(\frac{n-1}{n}\right)^b L^{-2(1-b)}, \tag{19}$$

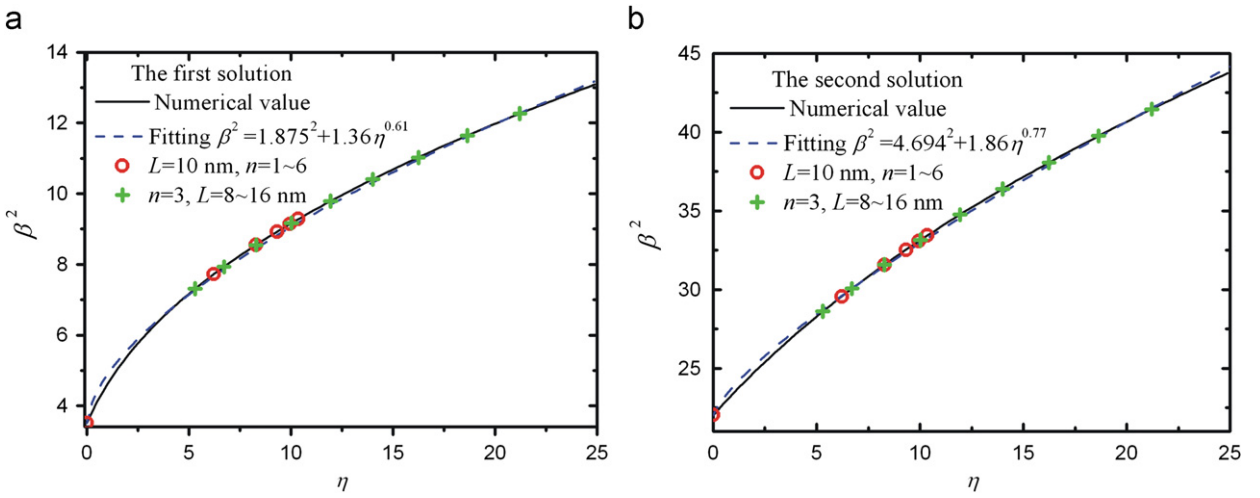

Fig. 4. The $\beta^2-\eta$ relationships of the fundamental and secondary solutions solved from Eq. (16). (a) The relationship of the fundamental solution, the red hollow circles correspond to fixed length $L=10$ nm and different layer number $n=1, 2, \ldots, 6$. The green crosses are for fixed layer number $n=3$ and different length $L=8, 9, \ldots, 16$. The dashed line is the least square fitting of the approximate relationship $\beta^2=\beta_0^2+a\eta^b$, with given $\beta_0=1.875$ and undetermined fitting constants a and b. (b) The $\beta^2-\eta$ relationship for the secondary solution, with the same representations as (a). (For interpretation of the references to color in this figure legend, the reader is referred to the web version of this article.)

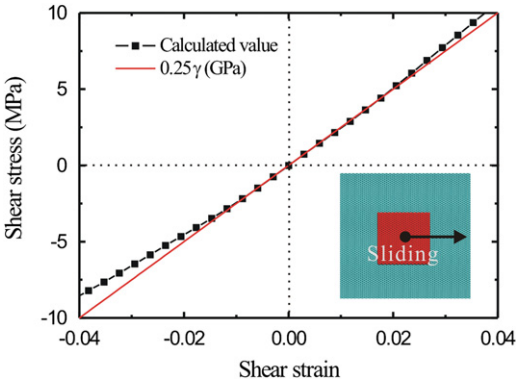

Fig. 5. Relationship between interlayer shear stress and strain of graphene layers, calculated by summing the van der Waals forces between a graphene flake and a substrate while the flake is sliding with respect to the substrate, with Lennard–Jones formula used. Linear fitting to the numerical results gives a shear modulus $G=0.25$ GPa.

where f_{mono} as given in Eq. (4) is the resonant frequency of monolayer graphene cantilever, and

$$k=\frac{a}{2\pi}\left(\frac{D_{\text{shear}}}{D_{\text{bend}}}\right)^b\sqrt{\frac{D_{\text{bend}}}{\rho h}}. \tag{20}$$

The only undetermined parameters involved in MBSM are the interlayer shear rigidity D_{shear} and the bending rigidity D_{bend} of monolayer graphene. We evaluate the bending rigidity D_{bend} through substituting the fundamental resonant frequency of monolayer graphene cantilever obtained in our MD simulation into the EBM frequency relationship Eq. (4). This gives $D_{\text{bend}}=3.42\times10^{-19}$ kg m^2 s^{-2}. To determine interlayer shear rigidity D_{shear}, which is defined as the product of interlayer shear modulus G and interlayer space h, we perform a MD numerical experiment, in which a small flake of single-layer graphene is sliding on a large single-layer graphene substrate and van der Waals forces between all atoms in the flake and the graphene substrate are calculated. The flake is a 5 nm-wide square and the substrate is a 15 nm-wide square that is large enough to eliminate the edge influence during sliding. The sliding direction is the same as what we observe in the vibration of multilayer graphene nanostrips, i.e. armchair direction. We use Lennard-Jones formula to represent the interlayer van der Waals interaction, with the formula and parameters all the same as used before for the interlayer interaction of Dreiding force-field (Mayo et al., 1990). In our calculation, the shear strain is defined as $\gamma=s/h$, where s is the displacement of the sliding graphene flake and h the graphene interlayer space. The calculated relationship between shear stress and strain is plotted in Fig. 5, from which we estimate shear modulus $G=0.25$ GPa by linearly fitting the curve in the range of small strains. With interlayer space $h=0.34$ nm, we obtain the shear rigidity of unit width $D_{\text{shear}}=0.085$ kg s^{-2}.

The blue dashed lines in Fig. 2 plot the MBSM prediction (Eq. (19)) of the fundamental and secondary resonant frequencies by using the above-determined values of D_{bend} and D_{shear}. Fig. 2(a) and (b) is the fundamental resonant frequencies of different layers and different lengths, respectively. Fig. 2(c) and (d) are for the secondary resonant frequencies. The results show an excellent agreement with the MD simulation results. The interlayer van der Waals interaction of the multilayer graphene nanostrips is very weak, so the interlayer shear deformation is remarkable during vibration. On the other hand the bending rigidity of single layer graphene is very small and the deflection of every layer in the multilayer graphene nanostrips is almost the same. In the MBSM model we assume that every layer graphene has the same deflection and account for the interlayer shear energy, so that it can accurately describe the vibration of the multilayer graphene nanostrips and predicts excellently the resonant frequencies.

4. Comparison with Timoshenko's model

Timoshenko's theory of beams provides a classical beam model that accounts for shear deformation. The eigen-equation for determining the resonant frequencies can be expressed into the following form (Salarieh and Ghorashi, 2006):

$$1+\frac{1}{2}\left(\frac{\alpha_+^2+\lambda_2^2}{\alpha_-^2-\lambda_2^2}+\frac{\alpha_-^2-\lambda_2^2}{\alpha_+^2+\lambda_2^2}\right)\cosh\alpha_-\cos\alpha_+-\frac{1}{2}\left(\frac{\alpha_+}{\alpha_-}-\frac{\alpha_-}{\alpha_+}\right)\sinh\alpha_-\sin\alpha_+=0, \tag{21}$$

where

$$\beta^2=\sqrt{\frac{\rho H}{D}}\omega L^2,$$
$$\lambda_1=\sqrt{\frac{\rho I}{D}}\omega L=\frac{H}{2\sqrt{3}}\frac{\beta^2}{L},$$
$$\lambda_2=\sqrt{\frac{\rho}{k_s G}}\omega L=\sqrt{\frac{D}{k_s G H}}\frac{\beta^2}{L}, \tag{22}$$

and

$$\alpha_\pm=\sqrt{\sqrt{\beta^4+\frac{1}{4}(\lambda_2^2-\lambda_1^2)^2}\pm\frac{1}{2}(\lambda_2^2+\lambda_1^2)}. \tag{23}$$

The shear coefficient k_s equals to 0.833 for the rectangular cross section.

In the Timoshenko's model the parameter λ_1 accounts for the effect of the cross section rotational inertia and the λ_2 accounts for the shear effect. If we do not consider these two effects, say that $\lambda_1=0$ and $\lambda_2=0$, and $\alpha_+=\alpha_-$, Eq. (21) degenerates into Eq. (2), i.e. the eigen-equation for EBM, so the Timoshenko's model degenerates to the EBM. However according to the definition of Eq. (23) α_+ is larger than α_-, so for the Timoshenko's model the sign of $\sinh\alpha_+\sin\alpha_-$ is

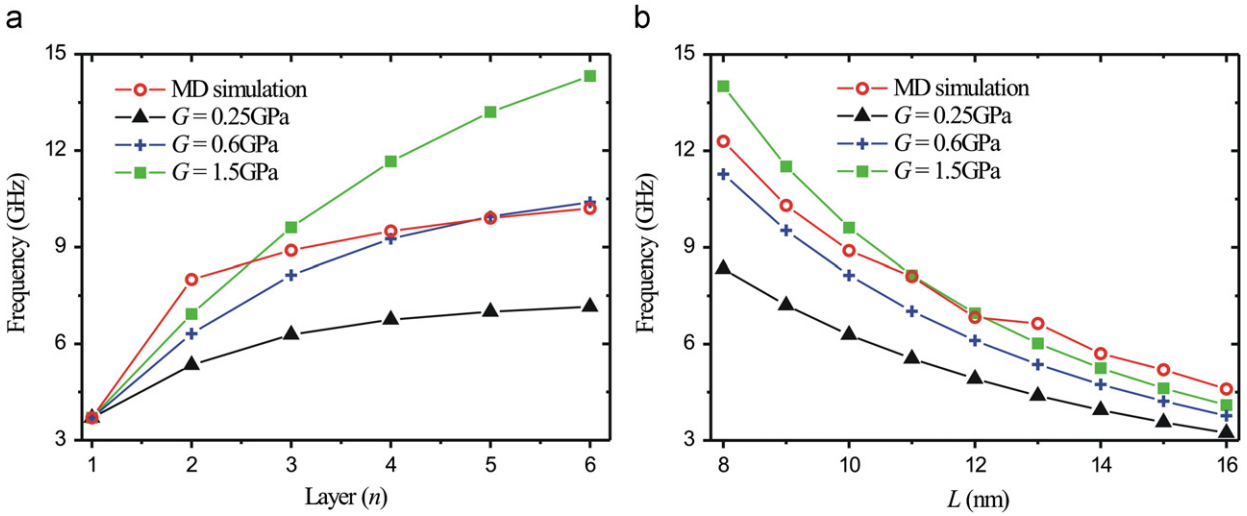

Fig. 6. Comparison of the fundamental resonant frequencies between the MD simulations (red hollow circles) and the Timoshenko's model predictions with respect to different shear modulus G=0.25 GPa (black triangles), G=0.6 GPa (blue crosses) and G=1.5 GPa (green squares). (a) Fixed nanostrip length L=10 nm and different layer number n=1, 2, …, 6. (b) Fixed layer number n=3 and different nanostrip length L=8, 9, …, 16 nm. (For interpretation of the references to color in this figure legend, the reader is referred to the web version of this article.)

always negative as in Eq. (21). This is different from the MBSM, so that the Timoshenko's model cannot degenerate to the MBSM even if we neglect the cross section rotational inertia effect $\lambda_1=0$.

As shown in Eqs. (22), the Timoshenko's model involves also two model parameters, the bending rigidity D per unit width and the shear modulus G. It is known that D is a cubic function of the beam height and is thus expressible as $D=D_{\text{bend}}n^3$ for n-layered graphene nanostrips, where D_{bend} denotes the bending rigidity of monolayer graphene nanostrip. We evaluate the same value $D_{\text{bend}}=3.42\times10^{-19}$ kg m^2 s^{-2} as obtained from the MD simulations. We then calculate the values of fundamental frequencies from the Timoshenko's model Eqs. (21) and (22) with respect to different values of the interlayer shear modulus G. Some results are plotted in Fig. 6. It is seen from Fig. 6 that the use of the previous $G=0.25$ GPa leads to a remarkable underestimate of the fundamental resonant frequencies for multilayer graphene cantilever nanostrips. It is also seen that the fundamental frequency as a function of layer number n and nanostrip length L cannot be simultaneously well predicted by adjusting a single material parameter G.

5. Closing remarks

In this work we find through molecular dynamics simulations that the resonant frequencies f of multilayer graphene cantilevers depend upon beam length L and layer number n in a manner very different from not only the classical Euler–Bernoulli prediction $f\propto nL^{-2}$, which is generally valid for thin beams, but also the Timoshenko's model prediction. Our MD simulation results can be described in the form $f-f_{\text{mono}}\propto[(n-1)/n]^bL^{-2(1-b)}$, where f_{mono} denotes the corresponding resonant frequency as the layer number is 1, with $b=0.61$ and 0.77 for the fundamental and secondary resonant models, where f_{mono} is the resonant frequency of a monolayer graphene cantilever.

It is also observed from MD simulated vibrations of the multilayer graphene cantilevers that interlayer shear occurs and all the layers have almost the same deflections. This is consistent with the known tremendous contrast between intralayer Young's modulus and interlayer shear modulus. Based on this observation, we propose the MBSM that gives excellent prediction agreeing well with MD simulations. The proposed MBSM includes only two parameters for material properties, i.e. bending rigidity D_{bend} of monolayer graphene sheet and interlayer shear rigidity D_{shear}. In our work, the value of D_{bend} is obtained by combining resonant frequency of monolayer graphene nanostrip from MD simulation with the predicted frequency expression from EBM $f_{\text{mono}}=(1.875^2/2\pi l^2)\sqrt{D_{\text{bend}}/\rho h}$, and D_{shear} is obtained by MD simulations, in which a graphene flake slides on a graphene substrate. The MBSM does not need any fitting parameter and makes prediction that agrees excellently with MD simulation results, implying that this model captures the intrinsic properties that define mechanics and dynamics of multilayer graphene nanostrips under bending.

From our MD simulations we find that during the bending of the multilayer graphene nanostrips, the interlayer shear deformation is remarkable due to the weak shear resistance. The EBM does not include this shear effect and fails here. The cross section of the multilayer graphene nanostrips is vertical and does not rotate during bending, thus the Timoshenko's model cannot work either. As evidenced by comparison with the MD simulation results, the MBSM proposed here accurately describes the deformation of the multilayer graphene nanostrips, and predicts excellently the resonant frequencies. Based on the analysis and discussion in this work, we would expect that the MBSM will also work for the mechanics and dynamics of other multibeam systems, such as the nanotube bundles.

Acknowledgments

Q.-S. Zheng acknowledges the financial supports from NSFC (Grant no. 10832005), the National Basic Research Program of China (Grant no. 2007CB936803) and the National 863 Project (Grant no. 2008AA03Z302). Z. Xu acknowledges NSFC Grant no. 11002079 for the support.

References

Arroyo, M., Belytschko, T., 2002. An atomistic-based finite deformation membrane for single layer crystalline films. Journal of the Mechanics and Physics of Solids 50, 1941–1977.

Arroyo, M., Belytschko, T., 2005. Continuum mechanics modeling and simulation of carbon nanotubes. Meccanica 40, 455–469.

Balandin, A.A., Ghosh, S., Bao, W.Z., Calizo, I., Teweldebrhan, D., Miao, F., Lau, C.N., 2008. Superior thermal conductivity of single-layer graphene. Nano Letters 8, 902–907.

Bao, W.Z., Miao, F., Chen, Z., Zhang, H., Jang, W.Y., Dames, C., Lau, C.N., 2009. Controlled ripple texturing of suspended graphene and ultrathin graphite membranes. Nature Nanotechnology 4, 562–566.

Bolotin, K.I., Sikes, K.J., Hone, J., Stormer, H.L., Kim, P., 2008. Temperature-dependent transport in suspended graphene. Physical Review Letters 101, 096802.

Bunch, J.S., van der Zande, A.M., Verbridge, S.S., Frank, I.W., Tanenbaum, D.M., Parpia, J.M., Craighead, H.G., McEuen, P.L., 2007. Electromechanical resonators from graphene sheets. Science 315, 490–493.

Chang, T., Gao, H., 2003. Size-dependent elastic properties of a single-walled carbon nanotube via a molecular mechanics model. Journal of the Mechanics and Physics of Solids 51, 1059–1074.

Chen, C.Y., Rosenblatt, S., Bolotin, K.I., Kalb, W., Kim, P., Kymissis, I., Stormer, H.L., Heinz, T.F., Hone, J., 2009. Performance of monolayer graphene nanomechanical resonators with electrical readout. Nature Nanotechnology 4, 861–867.

Cumings, J., Zettl, A., 2000. Low-friction nanoscale linear bearing realized from multiwall carbon nanotubes. Science 289, 602–604.

Ekinci, K.L., 2005. Electromechanical transducers at the nanoscale: actuation and sensing of motion in nanoelectromechanical systems (NEMS). Small 1, 786–797.

Ekinci, K.L., Yang, Y.T., Roukes, M.L., 2004. Ultimate limits to inertial mass sensing based upon nanoelectromechanical systems. Journal of Applied Physics 95, 2682–2689.
Fasolino, A., Los, J.H., Katsnelson, M.I., 2007. Intrinsic ripples in graphene. Nature Materials 6, 858–861.
Gómez-Navarro, C., Weitz, R.T., Bittner, A.M., Scolari, M., Mews, A., Burghard, M., Kern, K., 2007. Electronic transport properties of individual chemically reduced graphene oxide sheets. Nano Letters 7, 3499–3503.
Gibertini, M., Tomadin, A., Polini, M., Fasolino, A., Katsnelson, M.I., 2010. Electron density distribution and screening in rippled graphene sheets. Physical Review B 81, 125437.
Guo, Y., Karasawa, N., Goddard III, W.A., 1991. Prediction of fullerene packing in C60 and C70 crystals. Nature 351, 464–467.
He, X.Q., Kitipornchai, S., Liew, K.M., 2005. Buckling analysis of multi-walled carbon nanotubes: a continuum model accounting for van der Waals interaction. Journal of the Mechanics and Physics of Solids 53, 303–326.
Huang, X., Yuan, H., Liang, W., Zhang, S., 2010. Mechanical properties and deformation morphologies of covalently bridged multi-walled carbon nanotubes: multiscale modeling. Journal of the Mechanics and Physics of Solids 58, 1847–1862.
Huang, X.M.H., Zorman, C.A., Mehregany, M., Roukes, M.L., 2003. Nanodevice motion at microwave frequencies. Nature 421, 496.
Huang, Y., Wu, J., Hwang, K.C., 2006. Thickness of graphene and single-wall carbon nanotubes. Physical Review B 74, 245413.
Ke, C.H., Pugno, N., Peng, B., Espinosa, H.D., 2005. Experiments and modeling of carbon nanotube-based NEMS devices. Journal of the Mechanics and Physics of Solids 53, 1314–1333.
Kelly, B.T., 1981. Physics of Graphite. Applied Science Publishers.
Lee, C., Wei, X., Kysar, J.W., Hone, J., 2008. Measurement of the elastic properties and intrinsic strength of monolayer graphene. Science 321, 385–388.
Li, T., Zhang, Z., 2010. Substrate-regulated morphology of graphene. Journal of Physics D: Applied Physics 43, 075303.
Li, X., Zhu, Y., Cai, W., Borysiak, M., Han, B., Chen, D., Piner, R.D., Colombo, L., Ruoff, R.S., 2009. Transfer of large-area graphene films for high-performance transparent conductive electrodes. Nano Letters 9, 4359–4363.
Liew, K.M., He, X.Q., Kitipornchai, S., 2006. Predicting nanovibration of multi-layered graphene sheets embedded in an elastic matrix. Acta Materialia 54, 4229–4236.
Lindahl, E., Hess, B., van der Spoel, D., 2001. GROMACS 3.0: a package for molecular simulation and trajectory analysis. Journal of Molecular Modeling 7, 306–317.
Mayo, S.L., Olafson, B.D., Goddard III, W.A., 1990. Dreiding: a generic force field for molecular simulations. Journal of Physical Chemistry 94, 8897–8909.
Meyer, J.C., Geim, A.K., Katsnelson, M.I., Novoselov, K.S., Booth, T.J., Roth, S., 2007. The structure of suspended graphene sheets. Nature 446, 60–63.
Novoselov, K.S., Jiang, D., Schedin, F., Booth, T.J., Khotkevich, V.V., Morozov, S.V., Geim, A.K., 2005. Two-dimensional atomic crystals. Proceedings of the National Academy of Sciences of the United States of America 102, 10451–10453.
Poncharal, P., Wang, Z.L., Ugarte, D., de Heer, W.A., 1999. Electrostatic deflections and electromechanical resonances of carbon nanotubes. Science 283, 1513–1516.
Pugno, N., 2005. Tunneling current-voltage controls, oscillations, and instability of nanotube- and nanowire-based nanoelectromechanical systems. Glass Physics and Chemistry 31, 535–544.
Rivera, J.L., McCabe, C., Cummings, P.T., 2003. Oscillatory behavior of double-walled nanotubes under extension: a simple nanoscale damped spring. Nano Letters 3, 1001–1005.
Robinson, J.T., Burgess, J.S., Junkermeier, C.E., Badescu, S.C., Reinecke, T.L., Perkins, F.K., Zalalutdniov, M.K., Baldwin, J.W., Culbertson, J.C., Sheehan, P.E., Snow, E.S., 2010. Properties of fluorinated graphene films. Nano Letters 10, 3001–3005.
Robinson, J.T., Zalalutdinov, M., Baldwin, J.W., Snow, E.S., Wei, Z., Sheehan, P., Houston, B.H., 2008. Wafer-scale reduced graphene oxide films for nanomechanical devices. Nano Letters 8, 3441–3445.
Ru, C.Q., 2001. Axially compressed buckling of a doublewalled carbon nanotube embedded in an elastic medium. Journal of the Mechanics and Physics of Solids 49, 1265–1279.
Salarieh, H., Ghorashi, M., 2006. Free vibration of Timoshenko beam with finite mass rigid tip load and flexural–torsional coupling. International Journal of Mechanical Sciences 48, 763–779.
Shi, X., Cheng, Y., Pugno, N.M., Gao, H., 2010a. A translational nanoactuator based on carbon nanoscrolls on substrates. Applied Physics Letters 96, 053115.
Shi, X., Cheng, Y., Pugno, N.M., Gao, H., 2010b. Tunable water channels with carbon nanoscrolls. Small 6, 739–744.
Shi, X., Pugno, N.M., Cheng, Y., Gao, H., 2009. Gigahertz breathing oscillators based on carbon nanoscrolls. Applied Physics Letters 95, 163113.
Stankovich, S., Dikin, D.A., Dommett, G.H.B., Kohlhaas, K.M., Zimney, E.J., Stach, E.A., Piner, R.D., Nguyen, S.T., Ruoff, R.S., 2006. Graphene-based composite materials. Nature 442, 282–286.
Wang, L.F., Zheng, Q.S., 2007. Extreme anisotropy of graphite and single-walled carbon nanotubes bundles. Applied Physics Letters 90, 153113.
Wang, L.F., Zheng, Q.S., Liu, J.Z., Jiang, Q., 2005. Size dependence of the thin-shell model for carbon nanotubes. Physical Review Letters 95, 105501.
Xu, Z.P., 2009. Graphene nano-ribbons under tension. Journal of Computational and Theoretical Nanoscience 6, 625–628.
Xu, Z.P., Buehler, M.J., 2010. Geometry controls conformation of graphene sheets: membranes, ribbons, and scrolls. ACS Nano 4, 3869–3876.
Xu, Z.P., Zheng, Q.S., Jiang, Q., Ma, C.-C., Zhao, Y., Chen, G., Gao, H., Ren, G., 2008. Trans-phonon effects in ultrafast nano-devices. Nanotechnology 19, 255705.
Yakobson, B.I., Brabec, C.J., Bernholc, J., 1996. Nanomechanics of carbon tubes: instabilities beyond linear response. Physical Review Letters 76, 2511–2514.
Yu, M.F., Lourie, O., Dyer, M.J., Moloni, K., Kelly, T.F., Ruoff, R.S., 2000a. Strength and breaking mechanism of multiwalled carbon nanotubes under tensile load. Science 287, 637–640.
Yu, M.F., Yakobson, B.I., Ruoff, R.S., 2000b. Controlled sliding and pullout of nested shells in individual multiwalled carbon nanotubes. Journal of Physical Chemistry B 104, 8764–8767.
Zhang, Y.B., Tan, Y.W., Stormer, H.L., Kim, P., 2005. Experimental observation of the quantum Hall effect and Berry's phase in graphene. Nature 438, 201–204.
Zheng, Q.S., Jiang, B., Liu, S.P., Weng, Y.X., Lu, L., Xue, Q.K., Zhu, J., Jiang, Q., Wang, S., Peng, L.M., 2008. Self-retraction motion of graphite micro-flakes. Physical Review Letters 100, 067205.
Zheng, Q.S., Jiang, Q., 2002. Multiwalled carbon nanotubes as gigahertz oscillators. Physical Review Letters 88, 045503.